IEEE Transactions on Power Electronics

Universal Integrated Synchronization and Control for Three Phase DC/AC Converters

Journal:	*IEEE Transactions on Power Electronics*
Manuscript ID:	TPEL-Reg-2014-04-0619
Manuscript Type:	Regular Paper
Date Submitted by the Author:	24-Apr-2014
Complete List of Authors:	Karimi Ghartemani, Masoud; Mississippi State University, Electrical and Computer Engineering
Keywords:	

Universal Integrated Synchronization and Control for Three Phase DC/AC Converters

Masoud Karimi-Ghartemani, *Senior Member, IEEE*

Abstract

A methodology for operation of three phase DC/AC converters called the universal integrated control and synchronization (UISC) is proposed. The UISC is able to operate the inverter in grid-connected (GC) and stand-alone (SA) modes and seamless transition between these modes without reconfiguration of the control structure. It is, therefore, a desirable controller for the flexible micro-grid applications. The UISC provides independent control over real and reactive powers in GC mode and it performs voltage support in the SA mode. The UISC can operate for different filter structures (such as L, LC, and LCL) and is highly robust to the changes and uncertainties in the grid parameters. The UISC integrates the control and the synchronization tasks in a simple and compact structure which not only offers agile responses with minimum mutual dynamic, it is also well suited for digital implementations. The approach adopted by the UISC is fundamentally different from those widely adopted in converters based on the current control and/or voltage control methods. Its approach is rather from the same nature of those used in synchronous generators. This paper presents the UISC for three phase inverters and addresses theoretical aspects of it with accompanying numerical results.

Index Terms

Grid-connected converters, stand-alone converters, micro-grid, seamless transition, PLL, EPLL, current control, voltage control, droop control method, distributed generation.

The authors is with the Department of Electrical and Computer Engineering, Mississippi State University, Mississippi, USA. E-mail: karimi@ece.msstate.edu

Universal Integrated Synchronization and Control for Three Phase DC/AC Converters

I. Introduction

Microgrid (MG) is the key notion for the integration of distributed generation (DG) units, realization of combined heat and power (CHP) systems, reduction of transmission losses and transmission system expansions, increased availability and reliability of power and finally for the realization of smart grid objectives [1], [2]. Emerging technologies such as micro-turbine, solar photovoltaic (PV), fuel cell, gas internal combustion engine, and wind turbine systems require a power electronic inverter to convert the DC power to a stable and high quality AC power [3], [4]. Although the current practice does not allow islanding of a DG or a MG, the future electric power system (EPS) requires islanding operation [5]–[7].

As far as the control system requirements are concerned, a DG system is faced with different objectives when it operates in grid-connected (GC) mode or in stand-alone (SA) mode. In GC mode, the grid supplies the voltage and the DG is not supposed to participate in controlling the voltage. The DG simply supplies a power by supplying a current to the EPS. In this mode of operation, the DG may perform ancillary services such as reactive power compensation and harmonic filtering to some local loads [8]–[11]. Thus, a current control strategy is adopted in the control system of the DG [12]–[16]. In the SA mode and in a weak grid situation, however, the DG is supposed to participate in regulating the voltage profile across the MG nodes [1], [7] and normally a voltage control strategy is used [17]. A particular challenge is the seamless transition of the system between the GC and the SA modes. In transition from the GC to SA mode, the islanding is detected, the interface switch is turned off, and the control structure is reconfigured for the new mode. Undesirable transients may happen during the clearing time [18]. Before reconnecting to the grid, the inverter's output voltage is synchronized, the switch gets closed, and the control is reconfigured for the GC mode. A desirable feature of the DG control systems is the plug-and-paly property where the control system is as much independent as possible from the rest of the system. Ideally, this means that the DG control system should not depend on a communication link among the DGs and the rest of the system. Practically, some sort of low-bandwidth communication seems to be inevitable at least for some of the DGs, if not all of them, in a MG set-up.

The droop control method (DM) is well established with desirable features for controlling synchronous generators (SGs) through the governor and automatic voltage regulator (AVR) control systems [19], [20]. In a SG, the DM can operate the machine in both the GC and SA modes with no need to reconfiguration of control. There is even no need to detect the islanding of the machine. The governor and AVR set points will have different meanings in those different modes. In GC mode, those set points correspond to the real and reactive powers generated by the machine. In SA mode, they correspond to the magnitude and frequency of the machine's generated voltage. The DM has

been applied to parallel operation of uninterruptible power supply (UPS) systems [21], [22]. A widespread attempt is currently being made to adopt the DM for DGs as well. The DMs developed for electronically interfaced DGs, however, can hardly operate in both modes without need to reconfigure the control structure, in one way or another, when the system transfers from GC to SA or viceversa [18], [23]–[25]. There seems to be a fundamental difference between the conventional DM used in SGs and those developed for DGs. In the conventional DM used in SGs, the voltage and frequency (or speed) measurements are used to adjust the magnetic field and the input power of the machine. By these two variables, the internal induced voltage of the machine is adjusted. And the induced voltage impacts the actual output (or terminal) variable of the machine. In other words, there is no explicit control loop aimed at controlling the output variable of the machine (being current or voltage). In the DMs developed for DGs, on the contrary, there is consistently a voltage control loop aimed at controlling the output (or terminal) voltage [17], [26]–[31]. When the DG is connected to the grid, the output voltage is governed by the grid and the DG's voltage control loop fails to offer a sound and accurate control. Therefore, the control scheme needs to change mode from the voltage control to the current control. This is the root cause of the inconvenience. The situation may be mitigated if a large impedance (such as a transformer) exists in between the grid and the voltage terminals to be controlled [29], [32]–[35]. Methods based on adding virtual impedance are currently drawing much attention where derivatives of the output current are added in the control loop to emulate an output impedance [17], [27], [28], [36]–[40].

Another breed of control techniques for inverters are being introduced very recently that are based on attempts to mimic the SG control loops. The concepts of virtual SG (VSG) and virtual inertia [41]–[43], synchronverter [44], [45], and synchronous converter [46], [47] are some examples. These methods attempt to emulate the electromechanical and control subsystems of the SG. In general, these methods appear to offer superior performance compared to other existing methods. However, detailed analytical results and performance comparisons are still missing in the literature.

A universal control system with the following features is highly desirable for operation of a MG: 1) desired GC operation that is independent control over real and reactive powers, and high quality current; 2) desired SA operation that is regulated and high quality voltage profile across the MG nodes; 3) seamless transition from GC to SA mode that requires quick islanding detection or no need to islanding detection, and minimum or no reconfiguration of control structure; 4) seamless transition from SA to GC mode which requires synchronization, and minimum or no reconfiguration of control structure; 5) minimum (or no) communication link among the DGs and the rest of the system. This paper presents a new control system called the universal integrated synchronization and control (UISC) for three phase inverters to satisfy the above desired features. The UISC is based on direct extension of the conventional DM to the electronically interfaced DG systems. The UISC integrates the synchronization or the phase-locked loop (PLL) operation into its loop resulting in agility and robustness of responses as well as ease and robustness of digital implementations. The UISC was first presented in a single-phase application in [48]. This paper (i) expands the work of [48] to three phase applications, (ii) derives its stability margins, (iii) performs stability analysis for LCL output filter, (iv) performs stability analysis for SA operation in a multiple-inverter scenario, and

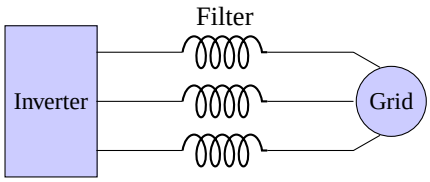

Fig. 1. Three-phase grid-connected inverter.

(v) presents further numerical test results pertaining to both the single-phase and three-phase applications.

II. Grid-Connected Operation

A. Developing ISC Method

Figure 1 shows the diagram for a three-phase grid-connected inverter. Assume that $v_g(t)$ and $v_{\rm inv}(t)$ denote the grid and inverter phase voltages, $i(t)$ denotes the current that flows from the inverter to the grid, and L denotes the interface filter inductance per phase. Thus,

$$v_{\rm inv}(t) = L\frac{di(t)}{dt} + v_g(t).$$

Define the virtual inverter voltage

$$v_i(t) = v_{\rm inv}(t) + Ri(t)$$

where R is a positive constant that emulates a resistor in series with L. Let the virtual inverter voltage phasor is denoted by $\overrightarrow{V_i} = V_i\angle\delta$ and the grid voltage phasor by $\overrightarrow{V_g} = V_g$ where V_i and V_g are the peak values; and δ is the phase angle. The virtual real and reactive powers at the inverter terminals are

$$P_i{=}\frac{3V_i}{2Z}[V_i\cos\theta - V_g\cos(\delta+\theta)],\ Q_i{=}\frac{3V_i}{2Z}[V_i\sin\theta - V_g\sin(\delta+\theta)]$$

where $\overrightarrow{Z} = R + jX = Ze^{j\theta}$, $X = L\omega$, and ω is the grid frequency in rad/s. Consider the transformation

$$T(\theta) = \begin{pmatrix} \sin\theta & -\cos\theta \\ \cos\theta & \sin\theta \end{pmatrix} = \frac{1}{Z}\begin{pmatrix} X & -R \\ R & X \end{pmatrix} \tag{1}$$

to define and calculate the transformed virtual powers as

$$\begin{pmatrix} P_i' \\ Q_i' \end{pmatrix} = T(\theta)\begin{pmatrix} P_i \\ Q_i \end{pmatrix} = \frac{3V_iV_g}{2Z}\begin{pmatrix} \sin\delta \\ \frac{V_i - V_g\cos\delta}{V_g} \end{pmatrix}. \tag{2}$$

In realistic, practical situations, the angle δ is small and, V_i is close to V_g. Consider, for example, a 10 kVA inverter with $L = 2$ mH and $R = 1$ connected to a 480 V (LL), 60 Hz line. When operating at extreme condition of $P_i' = 10$ k and $Q_i' = 0$, δ is about 3°. When operating at the other extreme condition of $P_i' = 0$ and $Q_i' = 10$ k, the relative distance of V_i to V_g is about 5%. Thus, it can be assumed that P_i' can chiefly be controlled by δ while

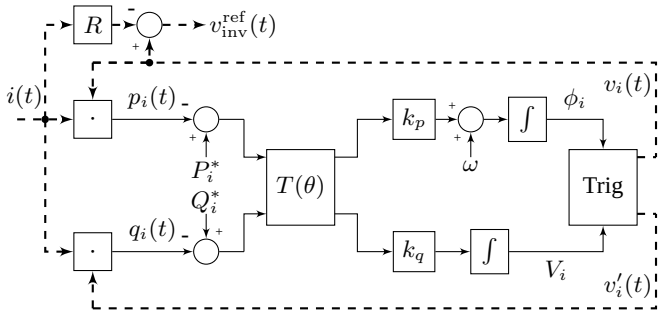

Fig. 2. Integrated synchronization and control (ISC) method.

Q_i' can be controlled by $V_i - V_g$. Based on this fact and assuming that $P_i'^*$ and $Q_i'^*$ are the reference values for those virtual powers, a control algorithm can be proposed as

$$\frac{\mathrm{d}}{\mathrm{dt}}V_i(t) = k_q(Q_i'^* - Q_i'), \quad \frac{\mathrm{d}}{\mathrm{dt}}\delta(t) = k_p(P_i'^* - P_i') \tag{3}$$

where k_p and k_q are some real positive constants.

In a balanced three phase system, the real and reactive powers P_i and Q_i are equal to the instantaneous real and reactive powers because the power ripples cancel out, that is

$$\begin{aligned} P_i &= p_i(t) = v_i(t)\cdot i(t) = v_{ia}(t)i_a(t) + v_{ib}(t)i_b(t) + v_{ic}(t)i_c(t) \\ Q_i &= q_i(t) = v_i'(t)\cdot i(t) = v_{ia}'(t)i_a(t) + v_{ib}'(t)i_b(t) + v_{ic}'(t)i_c(t) \end{aligned} \tag{4}$$

where $v_i{}'(t)$ is the 90° phase delayed version of $v_i(t)$ and $\cdot$ shows the dot product of two three phase vectors defined as $x \cdot y = x_1y_1 + x_2y_2 + x_3y_3$. Using (4), (3) can be represented in the matrix form as

$$\frac{\mathrm{d}}{\mathrm{dt}}\begin{pmatrix} \delta(t) \\ V_i(t) \end{pmatrix} = \begin{pmatrix} k_p & 0 \\ 0 & k_q \end{pmatrix} T(\theta) \begin{pmatrix} P_i^* - p_i(t) \\ Q_i^* - q_i(t) \end{pmatrix} \tag{5}$$

where $T(\theta)$ is defined in (1). Equation (5) summarizes the principles of the proposed grid-connected controller. A block diagram of this method is shown in Fig. 2 where the solid-thin lines show single-phase connections and the dashed-thick lines show three-phase connections. The "Trig" block calculates $v_i(t)$ and $v_i'(t)$ according to

$$v_i(t) = V_i \begin{pmatrix} \cos(\phi_i) \\ \cos(\phi_i - \frac{2\pi}{3}) \\ \cos(\phi_i + \frac{2\pi}{3}) \end{pmatrix}, \; v_i'(t) = V_i \begin{pmatrix} \sin(\phi_i) \\ \sin(\phi_i - \frac{2\pi}{3}) \\ \sin(\phi_i + \frac{2\pi}{3}) \end{pmatrix}. \tag{6}$$

The method of Fig. 2 integrates the synchronization and control tasks and we shall call it the integrated synchronization and control (ISC) method for three-phase grid-tie inverters.

B. Stability Analysis of the Control System

Theorem 1. Let $P_i^*{=}Q_i^*{=}0$, $k_q{=}\frac{k}{V_i}$ and $k_p{=}\frac{k}{V_i^2}$ for a constant k. Then, the ISC reduces to an LTI system.

Proof. Based on (6), define $x(t)$ as

$$x(t)=\begin{pmatrix} v_{ia}(t) \\ v'_{ia}(t) \end{pmatrix}=\begin{pmatrix} V_i\cos\phi_i(t) \\ V_i\sin\phi_i(t) \end{pmatrix}=V_i\begin{pmatrix} \cos\phi_i(t) \\ \sin\phi_i(t) \end{pmatrix}. \tag{7}$$

The differential equations of the system become

$$\dot{x}=\dot{V}_i\begin{pmatrix} \cos\phi_i \\ \sin\phi_i \end{pmatrix}+V_i\dot{\phi}_i\begin{pmatrix} -\sin\phi_i \\ \cos\phi_i \end{pmatrix}=\begin{pmatrix} -\sin\phi_i & \cos\phi_i \\ \cos\phi_i & \sin\phi_i \end{pmatrix}\begin{pmatrix} V_i\dot{\phi}_i \\ \dot{V}_i \end{pmatrix}. \tag{8}$$

Using (5), the latter vector can be written as

$$\begin{pmatrix} V_i\dot{\phi} \\ \dot{V}_i \end{pmatrix}=\begin{pmatrix} V_i\omega+V_i\dot{\delta} \\ \dot{V}_i \end{pmatrix}=\begin{pmatrix} V_i\omega \\ 0 \end{pmatrix}-V_i\begin{pmatrix} k_p & 0 \\ 0 & k_q \end{pmatrix}T(\theta)\begin{pmatrix} p_i(t) \\ q_i(t) \end{pmatrix}. \tag{9}$$

Substituting (9) in (8) and using (4), results in

$$\dot{x}(t)=\Omega x(t)-k\Theta i(t)$$

where

$$\Omega=\begin{pmatrix} 0 & -\omega \\ \omega & 0 \end{pmatrix},\ \Theta=\begin{pmatrix} \cos\theta & \cos(\theta+\frac{2\pi}{3}) & \cos(\theta-\frac{2\pi}{3}) \\ \sin\theta & \sin(\theta+\frac{2\pi}{3}) & \sin(\theta-\frac{2\pi}{3}) \end{pmatrix}.$$

This describes a second-order LTI system with input signal $i(t)$ and state vector $x(t)$. □

As far as the transfer function representation is concerned, it is observed that $v_{ia}(t)=Cx(t)$ where $C=(1,0)$, and hence

$$V_{ia}(s)=-kC(sI_2-\Omega)^{-1}\Theta_1 I(s) \tag{10}$$

where I_2 is the 2×2 identity matrix and Θ_1 is the first row of the matrix Θ. This transfer function can be expanded as

$$V_{ia}(s)=\frac{-kn_a(s)}{s^2+\omega^2}I_a(s)+\frac{-kn_b(s)}{s^2+\omega^2}I_b(s)+\frac{-kn_c(s)}{s^2+\omega^2}I_c(s) \tag{11}$$

where $n_a(s)=s\cos\theta-\omega\sin\theta,\ n_b(s)=s\cos(\theta+\frac{2\pi}{3})-\omega\sin(\theta+\frac{2\pi}{3}),\ n_c(s)=s\cos(\theta-\frac{2\pi}{3})-\omega\sin(\theta-\frac{2\pi}{3})$. Equations (10)-(11) represent the transfer function from the current signals to the phase-a virtual inverter voltage. Similar equations for phase-b and phase-c can be derived. This analysis shows that the overall closed-loop control system is a three-input three-output (3I3O) system (whose inputs are the current signals and whose outputs are the generated virtual inverter voltage signals and) whose matrix transfer function has non-zero values at all entries. It represents a coupled 3I3O system. In order to investigate the stability of the closed-loop system, it is noticed that a block diagram of the loop may be shown as in Fig. 3. This diagram shows the closed-loop system as far as phase-a is concerned. The term $c_p(t)$ lumps together the coupling terms that are forwarded from phase-b and phase-c loops.

The coupling terms do not change the stability of the closed-loop system but only impact its transient responses. The characteristic equation of the loop of Fig. 3 is equal to

$$1+k\frac{s\cos\theta-\omega\sin\theta}{(Ls+R)(s^2+\omega^2)}=0. \tag{12}$$

The root locus of this equation is shown in Fig. 4. The complex roots never become unstable. The real root is at

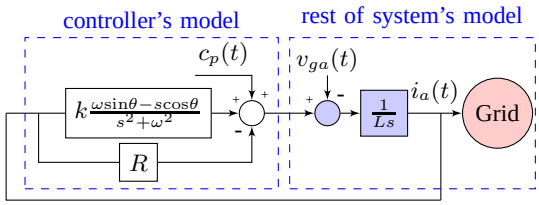

Fig. 3. Per-phase control block diagram of the closed-loop system.

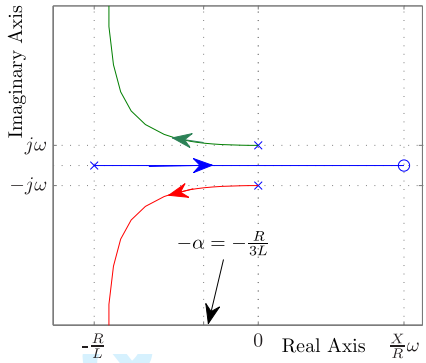

Fig. 4. Root-locus of the closed-loop control system of Fig. 3.

$-\alpha_0 = -\frac{R}{L}$ when $k = 0$ and it becomes unstable when $k > k_{\max}$ where

$$k_{\max} = \frac{R\omega}{\sin\theta} = R\omega\sqrt{1+(\frac{R}{L\omega})^2}. \tag{13}$$

The three roots will have equal real part of $-\alpha = -\frac{1}{3}\alpha_0 = -\frac{R}{3L}$ when $k = k_r$ where

$$k_{\rm r} = \frac{2}{3}R\omega\frac{Z}{X}\frac{3X^2+1/3R^2}{3X^2+R^2}. \tag{14}$$

This is the recommended value for k. An approximation of k_r may be given by $k_a = \frac{2}{3}R\omega$ which does not depend on L.

C. Design Algorithm

Given parameters: grid voltage and frequency, V_g, ω, and L.

Design parameters: k_p, k_q and R.

Step 1. Choose $\alpha > 0$. This directly corresponds to the transient speed of the system responses.

Step 2. Calculate R from $R = 3\alpha L$.

Step 3. Calculate k from $k = \frac{2}{3}R\omega$, or from (14).

Step 4. Calculate k_p and k_q from $k_p = \frac{k}{V_g^2}$ and $k_q = \frac{k}{V_g}$.

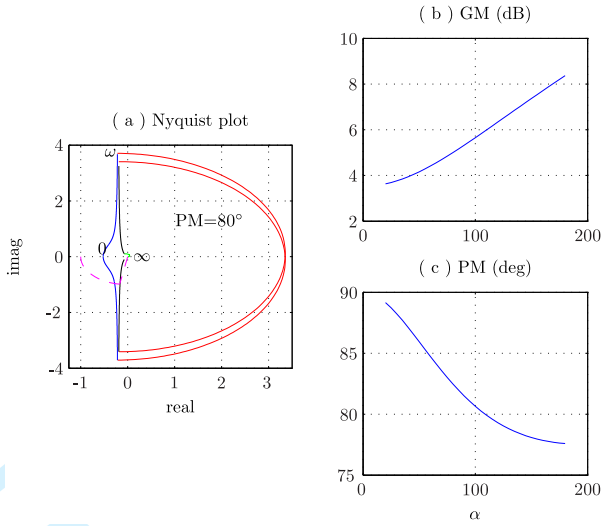

Fig. 5. Nyquist diagram, GM and PM of the closed-loop of Fig. 3

D. Stability Margins Analysis

Assume that the algorithm of Section II-C is used to design the controller gains based on $k = k_a$. The gain margin (GM) of the loop will be equal to

$$\text{GM} = \frac{k_{\max}}{k_a} = \frac{3}{2\sin\theta} = \frac{3Z}{2X} = \frac{3}{2}\sqrt{1+(\frac{3\alpha}{\omega})^2}. \tag{15}$$

This is drawn in Fig. 5(b) versus α. The system will have a GM of 4 dB to 8 dB for the values of α ranging in (40, 160).

To analyze the phase margin (PM) of the system, we notice from (12) that the open-loop transfer function is

$$k\frac{s\cos\theta-\omega\sin\theta}{(Ls+R)(s^2+\omega^2)} = \frac{2}{3}R\omega\frac{s\frac{3\alpha L}{\sqrt{9\alpha^2L^2+\omega^2L^2}}-\omega\frac{L\omega}{\sqrt{9\alpha^2L^2+\omega^2L^2}}}{(Ls+3\alpha L)(s^2+\omega^2)}$$

which simplifies to

$$\frac{2\alpha\omega}{\sqrt{w^2+9\alpha^2}}\frac{3\alpha s-\omega^2}{(s+3\alpha)(s^2+\omega^2)}. \tag{16}$$

The Nyquist diagram of this function for $\alpha = 100$ is shown in Fig. 5(a) which gives a GM of about 2 (6 dB) and a PM of about 80°. The PM versus the design parameter α is shown in Fig. 5(c). The system will have a PM varying in (87, 77) degrees for the values of α ranging in (40, 160).

Remark: Stability analysis of the proposed method with LCL output filter is presented in Appendix A where it is shown that the same design algorithm developed for L-filter is valid for LCL filter as well.

E. Frequency Updating

The proposed ISC method of Fig. 2 assumes that the grid frequency ω is given. It should be improved to estimate the frequency and adapt to its variations. The idea is similar to what is done in standard PLL and EPLL algorithms

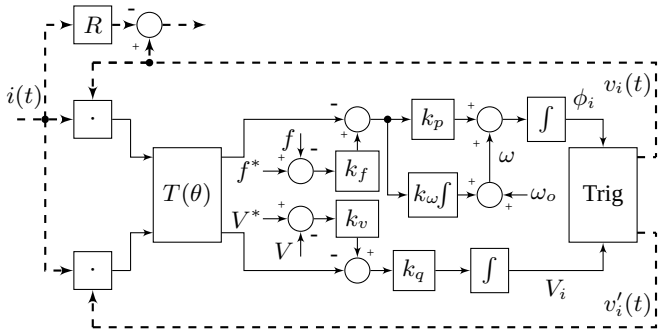

Fig. 6. Core UISC for both grid-connected and stand-alone operations.

[49] and is described by the differential equation

$$\dot{\Delta\omega}(t) = k_\omega(P_i'^* - P_i'), \quad \omega = \omega_o + \Delta\omega \tag{17}$$

where k_ω is a positive constant, ω_o is the nominal value of the system's frequency, and $\Delta\omega$ is the deviation of the actual frequency from the nominal value. The gain k_ω may be selected as $k_\omega = \frac{k'}{V_g^2}$ where $k' = \frac{1}{4\xi^2}k^2$ and ξ is a damping ratio with the recommended value in (1,5) [50], [51].

III. Grid-Connected and Stand-alone Modes

A. Developing UISC Method

In the SA operation, the converter supplies a local load or operates in conjunction with other converters within a micro-grid setup. The proposed ISC method, discussed in Section II, can be modified to operate in the SA mode as well. Inspired from the DM, modify (5) according to

$$P_i'^* = k_f(f^* - f), \; Q_i'^* = k_v(V^* - V) \tag{18}$$

where f^* and V^* are some set-points corresponding to a maximum frequency and voltage magnitude; k_f and k_v are real positive constants; and f and V are the actual output frequency and voltage magnitude. Then, (5) transforms to

$$\frac{\mathrm{d}}{\mathrm{dt}}\begin{pmatrix}\delta(t)\\ V_i(t)\end{pmatrix} = \begin{pmatrix}k_p & 0\\ 0 & k_q\end{pmatrix}\begin{pmatrix}k_f(f^*-f)-p_i'(t)\\ k_v(V^*-V)-q_i'(t)\end{pmatrix}. \tag{19}$$

Equation set (19) summarizes the core structure of the proposed universal ISC (UISC) controller whose block diagram is shown in Fig. 6. When the grid is available, f and V are equal (or very close) to f_o and V_o (the nominal values of frequency and voltage). Therefore, the inverter generates real and reactive powers equal to $P_i' = k_f(f^* - f_o)$ and $Q_i' = k_v(V^* - V_0)$, respectively. In the absence of grid, the inverter adjusts its real and reactive powers such that it satisfies

$$f = f^* - \frac{1}{k_f}P_i', \quad V = V^* - \frac{1}{k_v}Q_i'. \tag{20}$$

Equation set (20) is the conventional DM. Therefore, Fig. 6 automatically becomes the conventional DM in SA mode.

B. Stability Analysis of the Control System

As far as the SA operation is considered, two cases are distinguished and analyzed separately. Case I is when the inverter supplies a local load in the absence of other inverters. Case II is when multiple inverters operate in parallel. The following two theorems, whose proofs are provided in Appendix B, summarize the stability results.

Theorem 2. Consider the UISC and assume that the gains R, k_p, and k_q are selected according to II-C such that the GC operation is stable. The system retains its stability for SA mode supplying a single load regardless of the value of the load.

Theorem 3. Consider two inverters equipped with the UISC of Fig. 6 and assume that the gains R, k_p, and k_q are selected according to Theorem 1 and II-C such that both offer stable operation for GC mode. The aggregation of two inverters remain stable when disconnected from the grid and supplying a common load regardless of the value of the load.

Proof. See Appendix B for proof to these two theorems.

C. On Design of Parameters

Design of k_v, k_f, V^* and f^* can be done using the conventional droop principles and based on the inverter's power rating as well as the admissible ranges of voltage and frequency variations. Assume, for example, that S is the rated VA of the inverter and the inverter is supposed to operate at nominal voltage and frequency (V_o and f_o) when it delivers the rated power. The system's voltage and frequency can be as high as f^* and V^* when the real and reactive power approach zero. Thus, f^* and V^* are selected based on maximum admissible values of frequency and voltage, respectively. From there, k_v and k_f can be calculated as $k_v = \frac{S}{\Delta V}$, $k_f = \frac{S}{\Delta f}$ where $\Delta V = V^* - V_o$, $\Delta f = f^* - f_o$. The set-point parameters may also be determined through a secondary control mechanism that restores the frequency and magnitude of the voltage across the MG [52], [53].

D. Synchronization for Grid Connection

Before connecting to the grid, the voltage should be synchronized in order to avoid large transient currents. A synchronization strategy is shown in Fig. 7. A new branch is added to synchronize the two voltages $v_o(t)$ and $v_g(t)$. The cross product of $v_{o\alpha\beta}(t) \otimes v_{g\alpha\beta}(t) = v_{o\alpha}(t)v_{g\beta}(t) - v_{o\beta}(t)v_{g\alpha}(t)$ is proportional to the phase difference between the two voltages. If both voltages $v_o(t)$ and $v_g(t)$ are available at the inverter site (when the inverter is directly connected to the PCC, for example), the synchronization branch is implemented as part of the USIC. Otherwise, a low bandwidth communication system may be used to transmit the output of the cross product from the PCC to the inverter. In the latter case, the cross product is implemented at the PCC location and the UISC is implemented at the inverter site. At any rate, this branch generates a signal $\frac{3V_g^2}{2} k_\phi \sin(\phi_g - \phi_o)$. The suggested value for the gain k_ϕ is $\frac{2}{3V_g^2} nS$ where S is the rating of the inverter and n is a positive number whose suggested value is

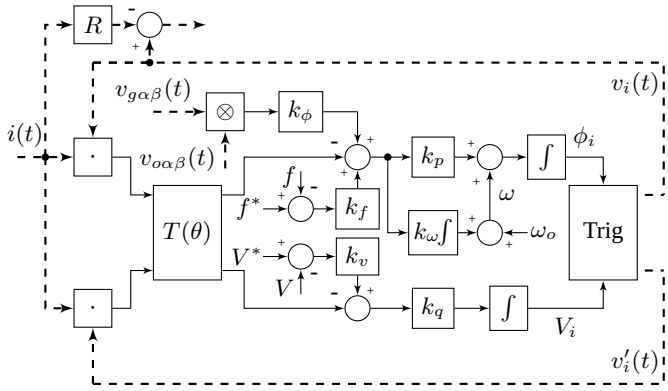

Fig. 7. Proposed UISC method for GC, SA, and seamless transition.

between 2 to 5. The larger the value of n, the higher and stronger the contribution of the inverter in synchronizing the two voltages.

IV. Numerical Results

A. System Description

Simulations are performed in PSIM [54] to present performance of the UISC in various operating conditions. The inverter has a three-leg topology with the dc voltage of 500 V. The output filter of the inverter is an LCL branch consisting of a $L_1 = 3$ mH, $L_2 = 2$ mH and $C = 8.3$ μF. The grid is a three-phase 208 V (line-to-line), 60 Hz. The load is a 1 kW, 0.5 kVar series RL load. The sinusoidal pulse-width modulation (SPWM) technique is used to generate the gating signals at a switching frequency of 10 kHz. The UISC of Fig. 7 is implemented in digital at the sampling frequency of 10 kHz. The current signal generated by the inverter, $i(t)$, is synchronously sampled to minimize the aliasing effect. The integrators are realized using the simplest method which is the first-order Euler forward integration: $y_n = y_{n-1} + T_s u_{n-1}$. The controller gains are $\alpha = 100,\ L = L_1 + L_2 = 0.005,\ R = 3\alpha L = 1.5,\ k = \frac{2}{3}\omega R = 377,\ k_q = \frac{k}{V_o} = \frac{377}{170} = 2.22,\ k_p = \frac{k}{V_o^2} = \frac{377}{170^2} = 0.013,\ k_\omega = \frac{k^2}{4\xi^2 V_o^2} = \frac{377^2}{16\times 170^2} = 0.31,\ k_f = \frac{S}{\Delta f} = \frac{2000}{2} = 1000,\ k_v = \frac{S}{\Delta V} = \frac{2000}{12\sqrt{2}} = 118,\ f^* = 60 + 2 = 62,\ V^* = (120 + 12)\sqrt{2} = 186.7,\ k_\phi = \frac{2}{3Vg^2} \times \frac{180}{\pi} \times 50 = 0.07.$

B. Scenario I: Single-Inverter

Scenario I is defined as follows.

1) Inverter starts at $t = 0$ s (no load, no grid).
2) Load is connected at $t = 0.1$ s.
3) Another identical load is connected at $t = 0.2$ s.
4) Load of 3) is disconnected at $t = 0.3$ s.
5) Grid is connected at $t = 0.4$ s.
6) f^* steps down to 61 at $t = 0.5$ s.

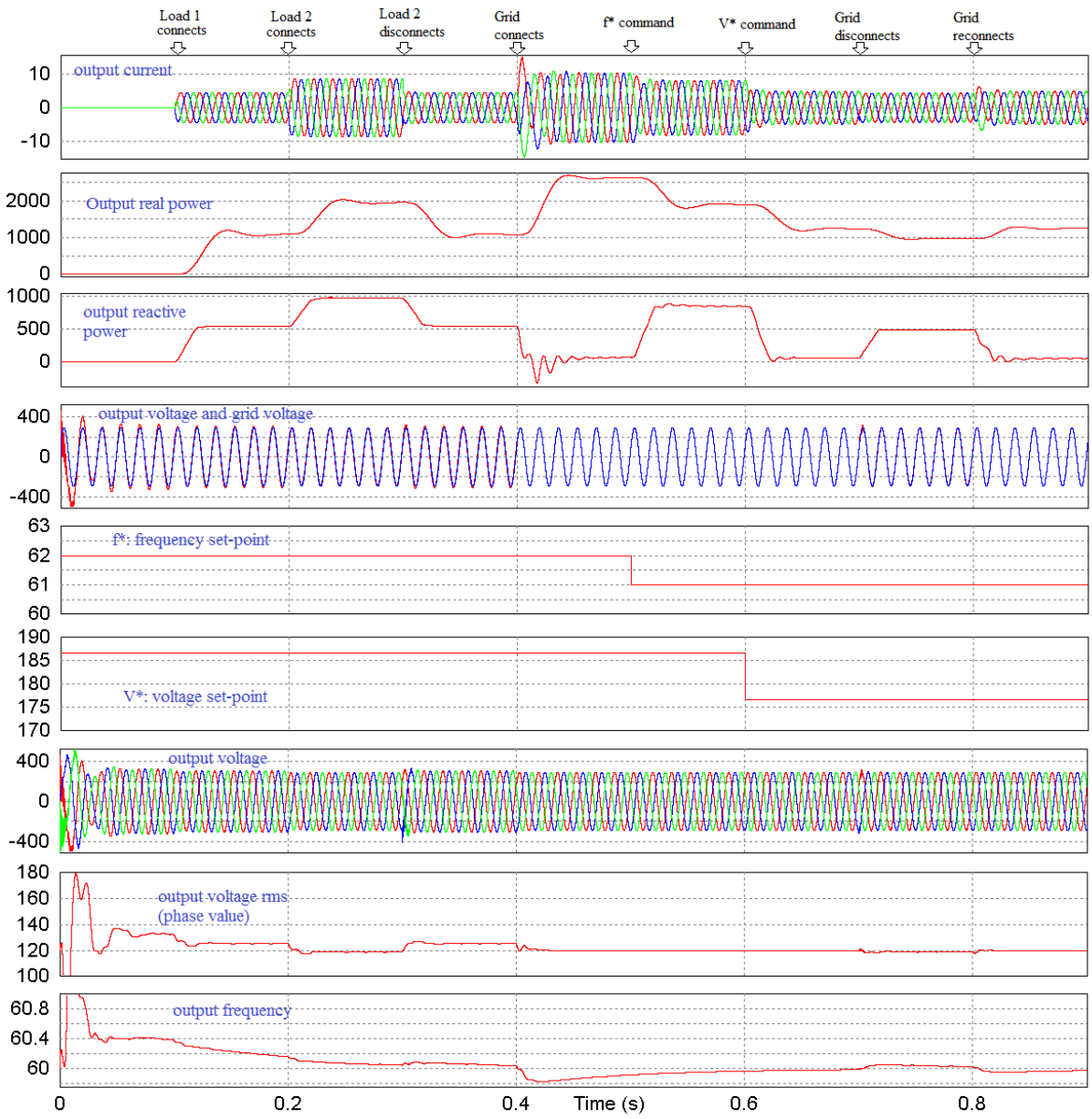

Fig. 8. Scenario I: system responses

7) V^* steps down to 176.7 at $t = 0.6$ s.

8) Grid is disconnected at $t = 0.7$ s.

9) Grid is reconnected at $t = 0.8$ s.

Responses of the system are shown in Fig. 8 respectively from top to bottom: the inverter output current (flowing through L_2); the real power generated at the actual output terminals of the inverter;; the reactive power generated at the actual output terminals of the inverter; the voltage at the output terminals of the inverter (only ab voltage) and

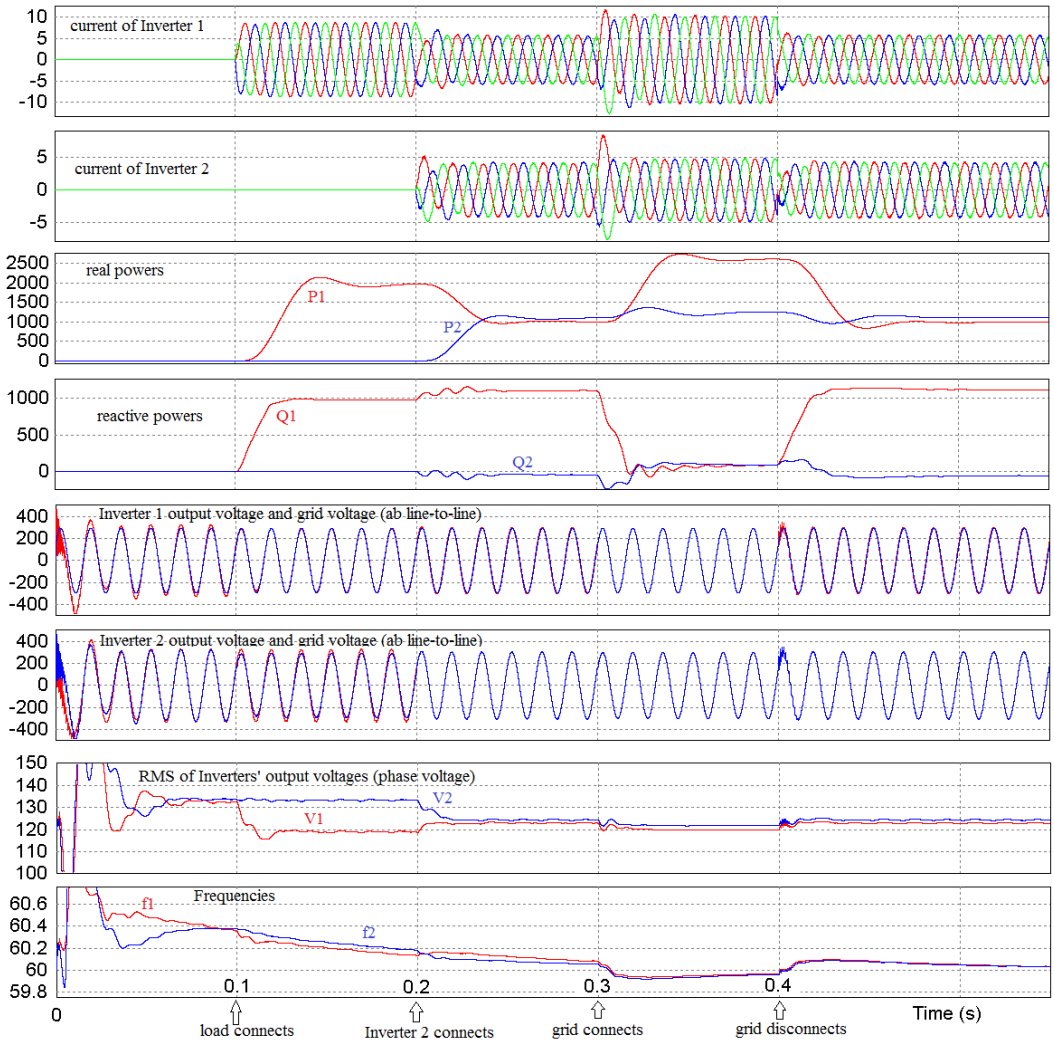

Fig. 9. Scenario II: System responses.

the corresponding grid voltage; frequency set-point f^*, voltage set-point V^*; line-to-line output voltages; rms of the inverter output voltage (phase voltage); and the frequency of the output voltage. In the intervals corresponding to the SA mode, $0 \leqslant t \leqslant 0.4$ s and $0.7 \leqslant t \leqslant 0.8$ s, the inverter supplies the load at a voltage and frequency close to the nominal values. The voltage regulation level of the inverter may be controlled by adjusting the two parameters V^* and f^*. During this mode, the inverter also synchronizes its output voltage with the grid voltage to become prepared for any sudden grid connection. During the intervals corresponding to the GC mode, $0.4 \leqslant t \leqslant 0.7$ s and $0.8 \leqslant t$ s, the inverter injects real and reactive powers to the grid. The amount of these two powers may be commanded by adjusting the two parameters V^* and f^* as observed from these two figures. The transitions between GC and SA modes are performed smoothly with no serious transients. The output voltage THD in SA mode as well as the output current THD in GC mode are about 0.5%. Desirable performance of the inverter is achieved.

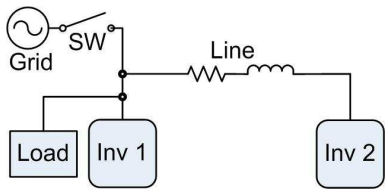

Fig. 10. Schematic of the micro-grid of Scenario II.

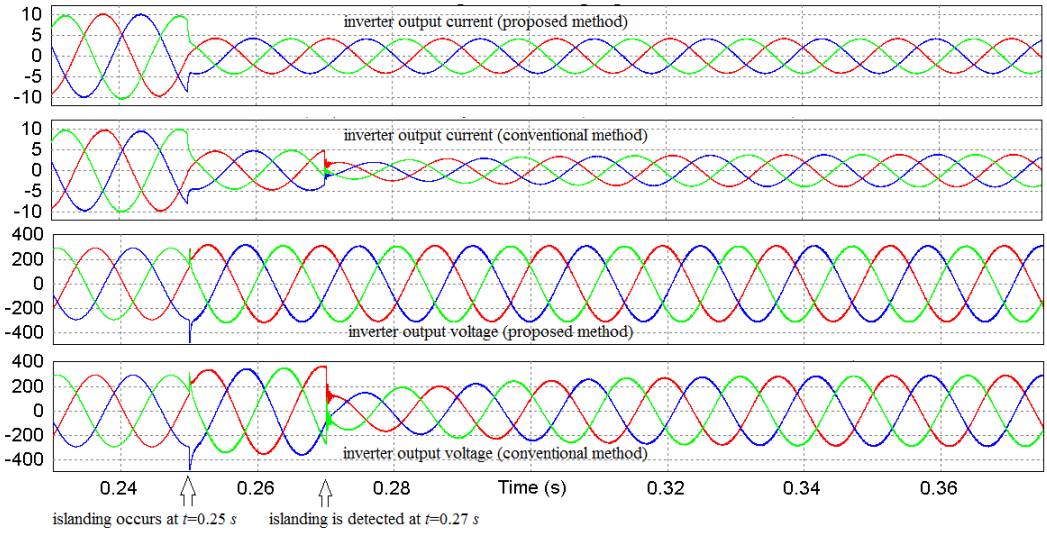

Fig. 11. Comparison of UISC and conventional method in transition from GC to SA.

C. Scenario II: Double-Inverter

In Scenario II, a micro-grid comprising of a 2 kVA inverter, a 1 kVA inverter, and a load of 2 kW, 1 kVar is considered, Fig. 10. The load is connected close to Inverter 1 where is also the point of coupling to the grid. Between the two inverters is a line with impedance of 0.5+j0.377 Ω. The grid parameters, and the inverters and their control system parameters follow the specifications described in Section IV-A. Each inverter is equipped with a switch at its point of connection to the network and it measures the voltages at both sides of this switch for the purpose of synchronization. Scenario II is defined as follows.

1) Both inverters start synchronizing at $t = 0$ s while Inverter 1 is connected to the bus and Inverter 2 is not. The grid is initially disconnected.

2) Load is connected at $t = 0.1$ s.

3) Inverter 2 is connected at $t = 0.2$ s.

4) Grid is connected at $t = 0.3$ s.

5) Grid is disconnected at $t = 0.4$ s.

Further cases such as change of f^* and V^* in SA mode (to control the voltage rms values) and in GC mode

(to control real and reactive powers) are not shown due to lack of space. Figure 9 shows responses of the system in the following order from top to bottom: output current of Inverter 1; output current of Inverter 2; output real powers of inverters; output reactive powers of inverters; output voltage of Inverter 1 and the grid voltage (line-to-line ab voltage); output voltage of Inverter 2 and the grid voltage (line-to-line ab voltage); rms value of inverters' output voltages; and frequencies. During $0 \leqslant t \leqslant 0.1$ s, Inverter 1 synchronizes to the grid voltage and Inverter 2 synchronizes to its own bus voltage. Inverters are smoothly switched into the network with very small and short transients. The transitions from GC to SA and vice versa are achieved seamlessly. The UISC offers desirable performance.

D. Comparison with Conventional Method

A conventional method based on using PR controllers for current control in GC mode and for voltage control in SA mode is simulated and its performance is compared against the proposed method in transition from GC to SA. Both systems are primarily operating in GC mode and each one injects about 2.5 kW real power and zero reactive power. Each inverter is also connected to a local load of about 1 kW. At time $t = 0.25$ s, the islanding occurs. It is assumed that the islanding detection algorithm for the conventional method takes 0.02 s. Therefore, assuming that the adjustable time and switch operating time [18] are neglected, the conventional method switches algorithm from current control to voltage control at $t = 0.27$ s. Simulation results are shown in Fig. 11. During $t = 0.25$ s and $t = 0.27$ s, the system is actually islanded while the control algorithm is still current control. Therefore, the grid power flows through the load and this causes a large over-voltage. After $t = 0.27$ s, the voltage control loop regulates the voltage after its transient period is over. Figure 11 shows that the conventional method cannot ensure a seamless transition from the GC to the SA mode. The proposed method offers a much superior performance.

E. Impact of Unbalance

Power quality issues in a MG are challenging research topics [55]. Performance of the UISC in the presence of unbalance load is investigated in this simulation. Initially, the UISC is supplying power to a balanced load of about 1000 W and 500 Var. At $t = 0.75$ s, a single-phase load is connected between two line-to-line terminals of the three-phase system. The impedance of this single-phase load is chosen equal to the value of the three-phase load (between the two lines). Figure 12 shows the inverter current, its output voltage and also the magnitude of the negative sequence voltage (line-to-line). Despite the highly unbalanced load, the voltage remains pretty much balanced. The negative sequence voltage is about 0.6% of the positive sequence for the balanced load and it is about 2.4% of the positive sequence for the highly unbalanced load. This simulation confirms desirable performance of the proposed method for unbalance load situations. It should also be mentioned that the proposed method can be extended to improve its performance against unbalanced load similar to the method presented in [56].

V. Conclusion

The universal integrated synchronization and control (UISC) is proposed to control operation of an electronically interfaced distributed generation (DG) system in grid-connected (GC) mode, stand-alone (SA) mode, and seamless

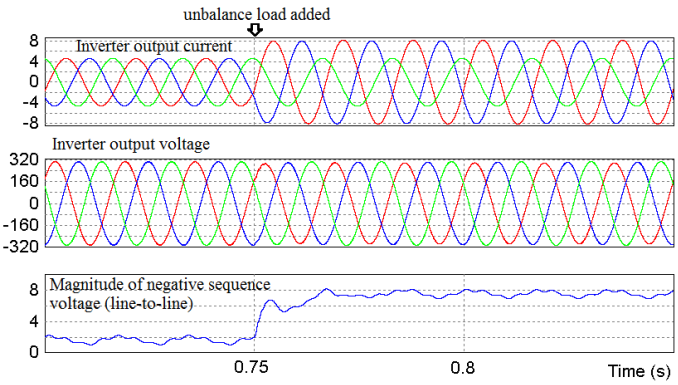

Fig. 12. Performance of the UISC against unbalanced load.

transition between the modes with no reconfiguration of control structure. The UISC is arguably the simplest structure ever presented to gain the entire features it offers. The integral structure comes with agility and robustness of responses which minimizes the possible adverse impacts of the DG on global transients of the electric power system or the microgrid.

APPENDIX A
LCL OUTPUT FILTER

The inductor-capacitor-inductor (LCL) output filter offers stronger attenuation of switching noises as compared with the L filter at a smaller inductor size. When the proposed method is used in an inverter with LCL output filter, the function $\frac{1}{Ls}$ is changed to $\frac{L_2Cs^2+1}{(L_1+L_2)s(L_{\rm eq}Cs^2+1)}$ where $L_{\rm eq}=L_1||L_2=\frac{L_1L_2}{L_1+L_2}$. Define the LCL transfer function as

$$H(s)=\frac{L_2Cs^2+1}{(L_1+L_2)s(L_{\rm eq}Cs^2+1)}=\frac{\frac{s^2}{\omega_z^2}+1}{Ls(\frac{s^2}{\omega_r^2}+1)}$$

where $\omega_r=\frac{1}{\sqrt{L_{\rm eq}C}}$ is the resonance frequency, $\omega_z=\frac{1}{\sqrt{L_2C}}$ and $L=L_1+L_2$. The LCL transfer function has two zeros at $\pm j\omega_z$, two resonance poles at $\pm j\omega_r$ and a single pole at origin. In order to perform the stability analysis, we divide it in two stages. First we investigate the effect of R on the closed-loop stability. Then the effect of other part that is $k\frac{s\cos\theta-\omega\sin\theta}{s^2+\omega^2}$ is studied.

The feedback branch R modifies the LCL transfer function to $H_R(s)=\frac{H(s)}{1+RH(s)}$ whose characteristic equation is

$$1+RH(s)=1+R\frac{\frac{s^2}{\omega_z^2}+1}{Ls(\frac{s^2}{\omega_r^2}+1)}=0. \tag{21}$$

As shown in Fig. 13(a), increasing R causes the real pole to move to the left and it also increases the damping of the resonance poles. Notice that only half of the complex plane is shown. Figure 13(a) shows the root-locus when R is increased from zero to infinity. Figure 13(b) shows the root-locus when R is increased from zero to $3\alpha L$.

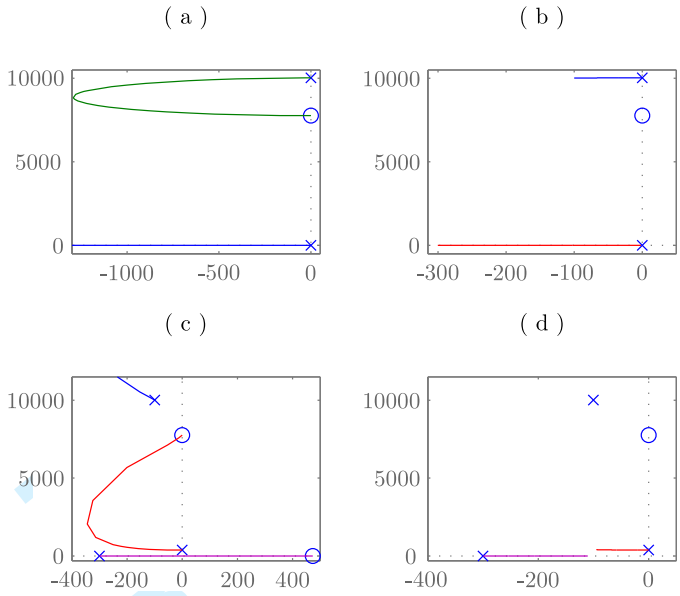

Fig. 13. Root-locus of the system with LCL filter

The characteristic equation of the complete loop is

$$1 + k\frac{s\cos\theta - \omega\sin\theta}{s^2+\omega^2}H_R(s) = 0. \tag{22}$$

The locus of the roots of this characteristic equation versus k is shown in Fig. 13(c) for k going from zero to infinity; and in Fig. 13(d) when k varies from zero to $k_a = \frac{2}{3}R\omega$. The loci shown in part (d) is very much close to the root-locus of the L filter shown in Fig. 4. Therefore, this concludes that the same controller designed for the L filter controls the LCL filter and offers similar transient responses. This is confirmed by numerical results.

APPENDIX B
STABILITY ANALYSIS IN SA MODE

Proof of Theorem 2. Using the results of Theorem 1, a simplified control block diagram of the system in this mode may be presented as Fig. 14. If $Z_L(s)$ denotes the load impedance, the closed-loop characteristic equation is

$$1 + \frac{k}{R + Ls + Z_L(s)}\frac{s\cos\theta - \omega\sin\theta}{s^2+\omega^2} = 0. \tag{23}$$

I. For a *series RL Load*, $Z_L(s) = L_1 s + R_1$, and (23) is

$$1 + \frac{k}{(R+R_1) + (L+L_1)s}\frac{s\cos\theta - \omega\sin\theta}{s^2+\omega^2} = 0 \tag{24}$$

which has the same form of the characteristic equation for the GC mode expressed by (12) and it has a similar root-locus to what is shown in Fig. 4. The maximum value of k which retains the stability is

$$k_{\max} = (R+R_1)\frac{\omega}{\sin\theta} = (R+R_1)\omega\sqrt{1+(\frac{R}{L\omega})^2} \tag{25}$$

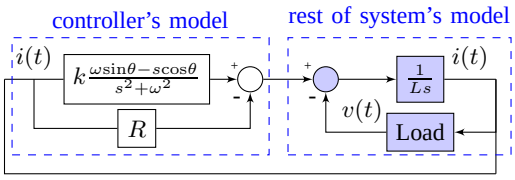

Fig. 14. Control block diagram in stand-alone mode: Case I.

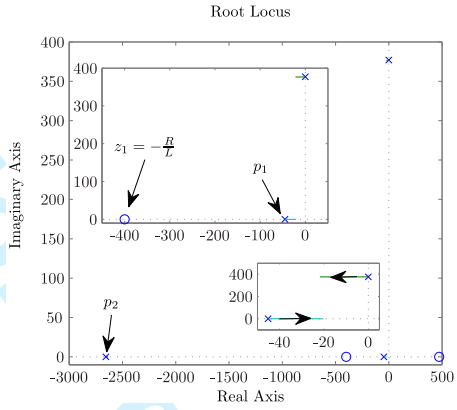

Fig. 15. Root-locus of single-inverter control system with a parallel RL load.

which is larger than the value for the GC mode given in (13). In other words, if the system is already designed for the GC mode to have a stable operation, it will surely maintain its stability for the SA operation as well. This result is also valid for the extreme cases of a purely resistive or a purely inductive load.

II. For a *parallel RL load*, $Y(s) = \frac{1}{Z(s)} = \frac{1}{R_1} + \frac{1}{L_1 s} = \frac{L_1 s + R_1}{R_1 L_1 s}$, and (23) becomes

$$1 + \frac{k(L_1 s + R_1)}{(Ls+R)(L_1 s+R_1)+R_1 L_1 s} \frac{s\cos\theta - \omega\sin\theta}{s^2+\omega^2} = 0. \tag{26}$$

The root-locus of (26) is drawn in Fig. 15 when k changes from zero to 400. The open-loop transfer function has two zeros at $z_1 = -\frac{R_1}{L_1}$ and $z_2 = \omega\tan\theta$. It has two poles at $\pm j\omega$, and two other poles $p_1,\ p_2$ which are the roots of $(Ls+R)(L_1 s+R_1)+R_1 L_1 s = 0$. Both p_1 and p_2 are stable for all values of R_1 and L_1. Moreover, p_1 is located on the right side of z_1 while p_2 is on the left side of $-\frac{R}{L}$. Interestingly enough, the maximum value of k that maintains the stability is given by $k_{\max} = \frac{R\omega}{\sin\theta}$ which is exactly equal to (13). In other words, the same design that ensures the stability of the GC control system, will maintain the stability of the SA control system regardless of the value of load.

Proof of Theorem 3. Figure 16 shows the control block diagram of the two-inverter system in SA mode. The analysis performed here assumes two identical inverters in terms of their filter inductances, control structures and values of control parameters. It can be shown that the characteristic equation of the loop of (16) is $\Delta(s) = \Delta_1(s)\Delta_2(s) = 0$ where $\Delta_1(s) = 0$ is the characteristic equation of the grid-connected loop given in (12) and $\Delta_2(s)$ is a slightly

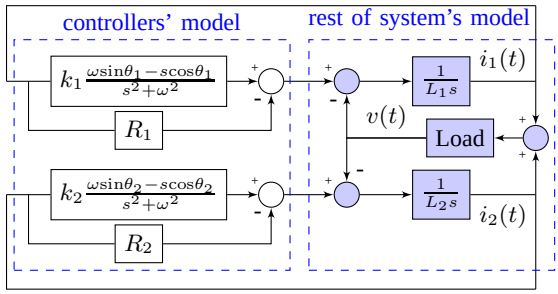

Fig. 16. Control block diagram in stand-alone mode (two inverters).

modified version of the characteristic equation of the stand-alone single-inverter system given in (26):

$$\Delta_2 = 1 + \frac{k(L_1 s + R_1)}{(Ls+R)(L_1 s + R_1) + 2R_1 L_1 s} \frac{s\cos\theta - \omega\sin\theta}{s^2+\omega^2}. \tag{27}$$

Form of the root-locus of (27) is similar to what is shown in Fig. 15 with the difference that the poles p_1 and p_2 are less stretched. The stability limit is also the same. Therefore, assuming that the single-inverter design for stand-alone is stable, the two-inverter loop will also be stable. The system has some fast modes (associated with $\Delta_1(s) = 0$) and some slow modes (associated with $\Delta_2(s) = 0$).

The above analysis method can be extended to the case where the two inverters are not identical. As such, it can be extended to multiple inverters. The analysis is systematic and can be easily developed into a computer program to perform the stability analysis for a general case.

REFERENCES

[1] R. H. Lasseter, "Smart distribution: Coupled microgrids," *Proceedings of the IEEE*, vol. 99, no. 6, pp. 1074–1082, 2011.

[2] B. Kroposki, R. Lasseter, T. Ise, S. Morozumi, S. Papatlianassiou, and N. Hatziargyriou, "Making microgrids work," *Power and Energy Magazine, IEEE*, vol. 6, no. 3, pp. 40–53, 2008.

[3] F. Blaabjerg, Z. Chen, and S. B. Kjaer, "Power electronics as efficient interface in dispersed power generation systems," *Power Electronics, IEEE Transactions on*, vol. 19, no. 5, pp. 1184–1194, 2004.

[4] R. H. Lasseter and P. Paigi, "Microgrid: a conceptual solution," in *Power Electronics Specialists Conference, 2004. PESC 04. 2004 IEEE 35th Annual*, vol. 6. IEEE, 2004, pp. 4285–4290.

[5] "IEEE1547 standard for interconnecting distributed resources with electric power systems," *IEEE Standards Coordinating Committee 21 on Fuel Cells, Photovoltaics, Dispersed Generation and Energy Storage*, pp. 1–27, 2003.

[6] "UL1741 standard for inverters, converters, controllers and interconnection system equipment for use with distributed energy resources," *Underwritters Laboratories Inc. Standard for Safety*, pp. 1–144, 2010.

[7] "IEEE P1547.4/D12 draft guide for design, operation, and integration of distributed resource island systems with electric power systems," *IEEE Standards Coordinating Committee 21 on Fuel Cells, Photovoltaics, Dispersed Generation and Energy Storage*, pp. 1–50, 2011.

[8] M. Prodanović, K. De Brabandere, J. Van den Keybus, T. Green, and J. Driesen, "Harmonic and reactive power compensation as ancillary services in inverter-based distributed generation," *IET Generation, Transmission & Distribution*, vol. 1, no. 3, pp. 432–438, 2007.

[9] A. Bracale, R. Angelino, G. Carpinelli, M. Mangoni, and D. Proto, "Dispersed generation units providing system ancillary services in distribution networks by a centralised control," *Renewable Power Generation, IET*, vol. 5, no. 4, pp. 311–321, 2011.

[10] R. I. Bojoi, L. R. Limongi, D. Roiu, and A. Tenconi, "Enhanced power quality control strategy for single-phase inverters in distributed generation systems," *Power Electronics, IEEE Transactions on*, vol. 26, no. 3, pp. 798–806, 2011.

[11] S. Dasgupta, S. K. Sahoo, S. K. Panda, and G. A. Amaratunga, "Single-phase inverter-control techniques for interfacing renewable energy sources with microgridpart II: Series-connected inverter topology to mitigate voltage-related problems along with active power flow control," *Power Electronics, IEEE Trans.*, vol. 26, no. 3, pp. 732–746, 2011.

[12] F. Blaabjerg, R. Teodorescu, M. Liserre, and A. Timbus, "Overview of control and grid synchronization for distributed power generation systems," *Industrial Electronics, IEEE Transactions on*, vol. 53, no. 5, pp. 1398–1409, Oct. 2006.

[13] A. Timbus, M. Liserre, R. Teodorescu, P. Rodriguez, and F. Blaabjerg, "Evaluation of current controllers for distributed power generation systems," *IEEE Trans. Power Elect.*, vol. 24, no. 3, pp. 654–664, 2009.

[14] B. Bahrani, A. Karimi, B. Rey, and A. Rufer, "Decoupled-current control of grid-tied voltage source converters using nonparametric models," *Industrial Electronics, IEEE Transactions on*, vol. 60, no. 4, pp. 1356–1366, 2013.

[15] B. Bahrani, M. Vasiladiotis, and A. Rufer, "High-order vector control of grid-connected voltage source converters with LCL-filters," *Industrial Electronics, IEEE Transactions on*, vol. 61, no. 6, pp. 2767–2775, 2014.

[16] R. Peña-Alzola, M. Liserre, F. Blaabjerg, M. Ordonez, and T. Kerekes, "Self-commissioning notch filter for active damping in three phase LCL-filter based grid-tie converter," *Power Electronics, IEEE Transactions on*, vol. DOI10.1109/TPEL.2014.2304468.

[17] J. Rocabert, A. Luna, F. Blaabjerg, and P. Rodriguez, "Control of power converters in ac microgrids," *Power Electronics, IEEE Transactions on*, vol. 27, no. 11, pp. 4734–4749, 2012.

[18] J. Kwon, S. Yoon, and S. Choi, "Indirect current control for seamless transfer of three-phase utility interactive inverters," *Power Electronics, IEEE Transactions on*, vol. 27, no. 2, pp. 773–781, 2012.

[19] P. Kundur, *Power system stability and control*. Tata McGraw-Hill Education, 1994.

[20] S. J. Chapman, *Electric machinery and power system fundamentals*. McGraw-Hill New York, 2002.

[21] J. M. Guerrero, L. GarciadeVicuna, J. Matas, M. Castilla, and J. Miret, "Output impedance design of parallel-connected UPS inverters with wireless load-sharing control," *Industrial Electronics, IEEE Transactions on*, vol. 52, no. 4, pp. 1126–1135, 2005.

[22] J. M. Guerrero, L. Hang, and J. Uceda, "Control of distributed uninterruptible power supply systems," *Industrial Electronics, IEEE Transactions on*, vol. 55, no. 8, pp. 2845–2859, 2008.

[23] R.-J. Wai, C.-Y. Lin, Y.-C. Huang, and Y.-R. Chang, "Design of high-performance stand-alone and grid-connected inverter for distributed generation applications," *Industrial Electronics, IEEE Transactions on*, vol. 60, no. 4, pp. 1542–1555, 2013.

[24] M. N. Arafat, S. Palle, Y. Sozer, and I. Husain, "Transition control strategy between standalone and grid-connected operations of voltage-source inverters," *Industry Applications, IEEE Transactions on*, vol. 48, no. 5, pp. 1516–1525, 2012.

[25] I. J. Balaguer, Q. Lei, S. Yang, U. Supatti, and F. Z. Peng, "Control for grid-connected and intentional islanding operations of distributed power generation," *IEEE Trans. Ind. Elect.*, vol. 58, no. 1, pp. 147–157, 2011.

[26] A. Bidram and A. Davoudi, "Hierarchical structure of microgrids control system," *Smart Grid, IEEE Transactions on*, vol. 3, no. 4, pp. 1963–1976, 2012.

[27] J. Kim, J. M. Guerrero, P. Rodriguez, R. Teodorescu, and K. Nam, "Mode adaptive droop control with virtual output impedances for an inverter-based flexible ac microgrid," *Power Electronics, IEEE Transactions on*, vol. 26, no. 3, pp. 689–701, 2011.

[28] J. M. Guerrero, J. C. Vasquez, J. Matas, M. Castilla, and L. G. de Vicuna, "Control strategy for flexible microgrid based on parallel line-interactive UPS systems," *Industrial Electronics, IEEE Transactions on*, vol. 56, no. 3, pp. 726–736, 2009.

[29] J. C. Vasquez, J. M. Guerrero, A. Luna, P. Rodríguez, and R. Teodorescu, "Adaptive droop control applied to voltage-source inverters operating in grid-connected and islanded modes," *Industrial Electronics, IEEE Transactions on*, vol. 56, no. 10, pp. 4088–4096, 2009.

[30] J. C. Vásquez Quintero, J. M. Guerrero Zapata, M. Savaghevi, R. Teodorescu *et al.*, "Modeling, analysis, and design of stationary reference frame droop controlled parallel three-phase voltage source inverters," *IEEE Trans. Ind. Elect.*, vol. 60, no. 4, pp. 1271–1280, 2013.

[31] J. M. Guerrero, J. C. Vasquez, J. Matas, L. G. de Vicuña, and M. Castilla, "Hierarchical control of droop-controlled ac and dc microgridsa general approach toward standardization," *Industrial Electronics, IEEE Transactions on*, vol. 58, no. 1, pp. 158–172, 2011.

[32] H. J. Avelar, W. A. Parreira, J. B. Vieira, L. C. G. de Freitas, and E. A. A. Coelho, "A state equation model of a single-phase grid-connected inverter using a droop control scheme with extra phase shift control action," *Industrial Electronics, IEEE Transactions on*, vol. 59, no. 3, pp. 1527–1537, 2012.

[33] R. A. Mastromauro, M. Liserre, T. Kerekes, and A. Dell'Aquila, "A single-phase voltage-controlled grid-connected photovoltaic system with power quality conditioner functionality," *Industrial Electronics, IEEE Transactions on*, vol. 56, no. 11, pp. 4436–4444, 2009.

[34] J. He, Y. W. Li, and M. S. Munir, "A flexible harmonic control approach through voltage-controlled DG–grid interfacing converters," *Industrial Electronics, IEEE Transactions on*, vol. 59, no. 1, pp. 444–455, 2012.

[35] J. He and Y. Li, "Hybrid voltage and current control approach for DG-grid interfacing converters with LCL filters," *Industrial Electronics, IEEE Transactions on*, vol. 60, no. 5, pp. 1797–1809, 2013.

[36] W. Yao, M. Chen, J. Matas, J. M. Guerrero, and Z.-M. Qian, "Design and analysis of the droop control method for parallel inverters considering the impact of the complex impedance on the power sharing," *Industrial Electronics, IEEE Transactions on*, vol. 58, no. 2, pp. 576–588, 2011.

[37] Y. W. Li and C.-N. Kao, "An accurate power control strategy for power-electronics-interfaced distributed generation units operating in a low-voltage multibus microgrid," *Power Electronics, IEEE Transactions on*, vol. 24, no. 12, pp. 2977–2988, 2009.

[38] J. Matas, M. Castilla, L. G. de Vicuña, J. Miret, and J. C. Vasquez, "Virtual impedance loop for droop-controlled single-phase parallel inverters using a second-order general-integrator scheme," *Power Electronics, IEEE Transactions on*, vol. 25, no. 12, pp. 2993–3002, 2010.

[39] J. M. Guerrero, P. C. Loh, M. Chandorkar, and T.-L. Lee, "Advanced control architectures for intelligent microgrids, part I: Decentralized and hierarchical control," *IEEE Transactions on Industrial Electronics*, vol. 60, no. 4, pp. 1254–1262, 2013.

[40] J. He, Y. Li, J. Guerrero, F. Blaabjerg, and J. Vasquez, "An islanding microgrid power sharing approach using enhanced virtual impedance control scheme," *Power Electronics, IEEE Transactions on*, vol. 28, no. 11, pp. 5272–5282, 2013.

[41] J. Driesen and K. Visscher, "Virtual synchronous generators," in *Power and Energy Society General Meeting-Conversion and Delivery of Electrical Energy in the 21st Century, 2008 IEEE*. IEEE, 2008, pp. 1–3.

[42] T. Shintai, Y. Miura, and T. Ise, "Oscillation damping of a distributed generator using a virtual synchronous generator," *Power Delivery, IEEE Transactions on*, vol. 29, no. 2, pp. 668–676, 2014.

[43] J. Alipoor, Y. Miura, and T. Ise, "Distributed generation grid integration using virtual synchronous generator with adoptive virtual inertia," in *Energy Conversion Congress and Exposition (ECCE), 2013 IEEE*. IEEE, 2013, pp. 4546–4552.

[44] Q.-C. Zhong and G. Weiss, "Synchronverters: Inverters that mimic synchronous generators," *Industrial Electronics, IEEE Transactions on*, vol. 58, no. 4, pp. 1259–1267, 2011.

[45] Q.-C. Zhong, P.-L. Nguyen, Z. Ma, and W. Sheng, "Self-synchronized synchronverters: Inverters without a dedicated synchronization unit," *Power Electronics, IEEE Transactions on*, vol. 29, no. 2, pp. 617–630, 2014.

[46] M. Ashabani and Y. Abdel-Rady I. Mohamed, "Novel comprehensive control framework for incorporating vscs to smart power grids using bidirectional synchronous-vsc," *Power Systems, IEEE Transactions on*, vol. 29, no. 2, pp. 943–957, 2014.

[47] ——, "New family of microgrid control and management strategies in smart distribution gridsanalysis, comparison and testing," *Power Systems, IEEE Transactions on*, vol. Digital Object Identifier 10.1109/TPWRS.2014.2306016.

[48] M. Karimi-Ghartemani, "Universal integrated synchronization and control for single phase dc/ac converters," *Power Electronics, IEEE Transactions on*, vol. Digital Object Identifier: 10.1109/TPEL.2014.2304459.

[49] M. Karimi-Ghartemani and M. Iravani, "A nonlinear adaptive filter for online signal analysis in power systems: applications," *Power Delivery, IEEE Transactions on*, vol. 17, no. 2, pp. 617–622, 2002.

[50] M. Karimi-Ghartemani and J. A. Walseth, "Using the epll algorithm as a preprocessor for fault analysis," in *Information Science, Signal Processing and their Applications (ISSPA), 2012 11th International Conference on*. IEEE, 2012, pp. 1377–1382.

[51] M. Karimi-Ghartemani, "Linear and pseudo-linear enhanced phased-locked loop (EPLL) structures," *Industrial Electronics, IEEE Transactions on*, vol. PP, no. 99, p. 1, 2013.

[52] T. Vandoorn, J. Vasquez, J. De Kooning, J. Guerrero, and L. Vandevelde, "Microgrids: Hierarchical control and an overview of the control and reserve management strategies," *Industrial Electronics Magazine, IEEE*, vol. 7, no. 4, pp. 42–55, 2013.

[53] Q. Shafiee, J. M. Guerrero, and J. C. Vasquez, "Distributed secondary control for islanded microgrids - a novel approach," *Power Electronics, IEEE Transactions on*, vol. 29, no. 2, pp. 1018–1031, 2014.

[54] PSIM, "Software by powersim technologies," *Professional Version*.

[55] J. M. Guerrero, P. C. Loh, T.-L. Lee, and M. Chandorkar, "Advanced control architectures for intelligent microgridspart II: Power quality, energy storage, and AC/DC microgrids," *Industrial Electronics, IEEE Transactions on*, vol. 60, no. 4, pp. 1263–1270, 2013.

[56] M. Savaghebi, A. Jalilian, J. C. Vasquez, and J. M. Guerrero, "Autonomous voltage unbalance compensation in an islanded droop-controlled microgrid," *Industrial Electronics, IEEE Transactions on*, vol. 60, no. 4, pp. 1390–1402, 2013.